Proceedings of ASME Turbo Expo 2024
Turbomachinery Technical Conference and Exposition
GT2024
June 24-28, 2024, London, United Kingdom

GT2024-126934

A HOLISTIC CONCEPTUAL SYNTHESIS AND ANALYSIS OF FUEL CELL SYSTEM ARCHITECTURES USING 1D COUPLED THERMOFLUID AND ELECTROCHEMICAL LUMPED PARAMETER SYSTEM SIMULATION

Vlad Goldenberg
SoftInWay, Inc.
Burlington, MA, USA

Ben Conser
SoftInWay, Inc.
Burlington, MA, USA

Clement Joly
SoftInWay, Inc.
Burlington, MA, USA

Leonid Moroz
SoftInWay, Inc.
Burlington, MA, USA

ABSTRACT

In this work, several fuel cell system architectures are described and analyzed. The architecture variability includes uncoupled/coupled cooling and aspirant systems, the inclusion or exclusion of an energy recovery turboexpander on the exhaust, and, for those that include a turboexpander, the inclusion or exclusion of thermal recuperation.

It is recognized a-priori that certain architectures will have specific advantages over others. It is also recognized that there are several performance metrics that may be sought. They include power system efficiency, gravimetric power density, volumetric power density, and specific cost per capacity. The analyses carried out in this work lead to a novel way to minimize the cost of a fuel cell power system. Specifically, knowing that the fuel cell proper represents the highest cost component of a fuel cell based power system, it is shown that one can optimize for maximum "bang for the buck" in a surrogate fashion in a holistic system analysis. The key to being able to achieve this is having a reliable electrochemical analysis model of a cell coupled with an overall system simulation model. Thus, for a variation of parameters, it can be predicted how relative fuel cell stack specific power density changes with parameter variation. The outcome of this paper is a documentation of several integrated fuel cell system architectures with a parametric analysis and resulting performance metrics of each system when independently optimized for efficiency, power density, and fuel cell specific power capacity, showing an improvement of about 15% over a simple baseline.

Keywords: Fuel Cell, Hydrogen, System Analysis

NOMENCLATURE

ϕ	Fuel-Air Equivalence Ratio
SA	Simply Aspirated
PRNR	Pressure Recovery Non-Recuperated
PRHR	Pressure Recovery Hot Recuperated
PRCR	Pressure Recovery Cold Recuperated
ITMR	Integral Thermal Management Recuperated
PEM	Proton Exchange Membrane
MEA	Membrane Electrode Assembly
ACS	Auxiliary Cooling System
SIC	Specific Investment Cost
BOP	Balance of Plant
N_{cell}	Cells Number
I	Current
U, V	Voltage
U_{act}	Activation losses
U_{ohm}	Ohmic losses
U_{conc}	Concentration losses
E	Cell Potential
E_0	Ideal Open Circuit Potential
i	Current Density
i_0	Exchange Current Density
A	Fuel Cell Area
α_c	Catalyst-Specific Area
L_c	Catalyst Loading
λ	Membrane Humidity
m_{H2}	Mass content of hydrogen at the fuel inlet
m_{ox}	Mass content of oxygen at the air inlet
ΔG	Gibbs free energy change
ΔH	Enthalpy change
ΔS	Entropy change
r_H	Number of protons passing through the membrane
F	Faraday's constant
μ_{H2}	Molar Mass of Hydrogen
r_m	Membrane Specific Resistance
l	Membrane Thickness
R_m	Membrane Resistance
η_{FC}	Fuel Cell Efficiency
$\dot{W}_{elec}$	Electrical Power
$\dot{W}_{chem}$	Chemical Power
H_{chv}	Hydrogen Calorific Heating Value

1. INTRODUCTION

Fuel cells are an important piece of the power and propulsion system matrix that may enable the decarbonization of power generation, transportation, and other industries. This decarbonization statement, of course, presupposes that the hydrogen, which is known to be an energy carrier rather than source, is produced from renewable sources. The primary methods of converting the hydrogen fuel back into useable energy are either using a heat engine to generate mechanical work or in a fuel cell to directly generate electrical power. The most promising candidates of a heat engine for using hydrogen as fuel are reciprocating internal combustion engines and gas turbines. Both technologies are compatible with traditional fuels and are therefore highly advanced after more than a century of development. In simple cycle mode, such engines can practically achieve an efficiency of 41%, while in combined cycle mode that uses a waste heat recovery bottoming cycle efficiencies of slightly over 60% [1] are achievable at the expense of high complexity, mass, and volume. Fuel cells typically achieve high efficiencies in direct power conversion of 40%-80%, with efficiencies of 60% quite typical [2]. Thus, their first advantage is high efficiencies that are not limited by Carnot limits (they are not heat engines). Additionally, the high combustion temperatures necessary to achieve high efficiencies in heat engines results in the formation of oxides of nitrogen (NO_x) when air, rather than pure oxygen, is used. NO_x is a serious polluter; therefore, a second important advantage of fuel cells is the clean exhaust. Finally, the mechanical equipment in heat engines tends to force the cycle toward lower efficiencies at partial load. On the other hand, the fuel cell stack fundamentally increases in efficiency when current draw is reduced [3], and although the air supply subsystem is a mechanical component whose parasitic loss may increase as a percentage of total power, it may be offset by the higher stack efficiency. Consequently, under the right conditions fuel cell systems can be designed such that the power system maintains high efficiency across the load range and is therefore suitable for applications requiring robust range control. There are also distinct disadvantages of fuel cells that must be acknowledged. The first is simply power density and specific power. Aside from solid oxide fuel cells (SOFC), which may have power densities and specific power capabilities that are competitive with gas turbines [4], the current state of the art in proton exchange membrane fuel cells (PEMFC) has both parameters as approximately an order of magnitude less than gas turbines. The second disadvantage that is of prime concern to this study is the high cost of fuel cell power systems. The fuel cell stack is the singular most expensive component, representing approximately 75% of the overall system cost [5]. The reason of the high cost is the catalyst and intricate nature of the membrane electrode assembly (MEA). In estimated volume manufacturing, about 60% of the cost is indeed the catalyst material [5]. Since almost half the capital cost of the fuel cell is attributed to the rare catalyst material, it is desired to optimize the design of fuel cell based power systems such that maximum power output capacity can be gained per fuel cell stack expenditure. The system simulations performed in this work are intended to document conceptual system architectures which achieve the goal to various degrees.

It is recognized that some architectures, while maximizing the specific power on the stack mass basis, may not maximize system specific power or power density, as the BOP equipment may account in some cases for the majority of the mass and/or volume of a particular system. Thus, certain applications, particularly in aerospace, may not be tolerant of a low system specific power to save on capital cost. However, many applications exist where overall system weight and volume are not so critical, and cost drives the difference between niche application and industry-wide adoption.

It is acknowledged that fuel cell models have been generated previously as part of other publications. Certain publications focus on just modeling the fuel cell parameters and its performance [3], [6], [7], [8]. Other publications couple the fuel cell model with other system models such as a vehicle system [9], [10] or rotorcraft system [11]. Several fuel cell system optimization studies have been performed based on optimizing different system parameters [12]. This includes optimizing systems based on power density through the variation of physical fuel cell parameters [13] or heat exchanger parameters for a SOFC-GT hybrid cycle [14]. What differentiates our study is that we are incorporating a PEMFC model with an overall system model and varying the system configuration and operating condition to better understand how to extract the most net system power for a fixed PEMFC stack geometry or parameter set.

2. METHODS

2.1 Analytical Methods

The analysis for this work was performed in a coupled 0D/1D system simulation commercial program called AxSTREAM System Simulation. Here, 0D refers to components that are defined by performance parameters, whereas 1D refers to components whose performance parameters are calculated within the model by either fundamental physical rules or empirical correlations, or some hybrid of the two. A 1D model of a PEMFC was developed and used in this work. This model was implemented using the AxSTREAM System Simulation software. The 1D model [15] has been in development for several years, was enhanced during the course of this work, and will continue fidelity enhancement because it is integrated into the commercial thermofluid system simulation software AxSTREAM System Simulation, which is continuously enhanced with the feedback of industry and customer needs. The model builds upon the foundation of previous PEMFC models [3], [6]. Several fuel cell parameters were accounted for when modelling the PEM fuel cell. These physical parameters include the fuel cell area (A), catalyst specific area (α_c), catalyst loading (L_c), membrane humidity (λ), membrane thickness (l), and number of cells (N_{cell}). As part of the analysis, several of these parameters were allowed to vary to see their effect on specific cell electrical power density for a fixed current density. Important equations that define the 1D model are presented below. This is not intended to be an exhaustive model definition.

The reader is referred to reference [15] and supplementally, [3] and [6] for a complete model description.

$$I = \frac{r_H F}{N_{cell}} = \left(\frac{2MFR_{H_2} m_{H_2} Util_{H_2}}{\mu_{H2}}\right)\left(\frac{F}{N_{cell}}\right) \quad (1)$$

$$E = E_0 + \frac{RT}{nF}\ln\left(\frac{P_{H_2} P_{O_2}^{0.5}}{P_{H_2O}}\right) \quad (2)$$

$$U = U_{cell} N_{cell} = (E - U_{act} - U_{ohm} - U_{conc}) N_{cell} \quad (3)$$

$$U_{act} = -\frac{RT}{\alpha_c F}\ln\left(\frac{i}{i_0}\right) \quad (4)$$

$$U_{ohm} = IR_m = \frac{Ir_m l}{A} \quad (5)$$

$$U_{conc} = c \cdot e^{\frac{i}{d}} \quad (6)$$

$$r_m = \frac{181.6\left(1+0.03\cdot\left(\frac{i}{A}\right)+0.062\cdot\left(\frac{T}{303}\right)^2\cdot\left(\frac{i}{A}\right)^{2.5}\right)}{\left(\lambda-0.634-3\left(\frac{i}{A}\right)\right)\exp\left(\frac{4.18(T-303)}{T}\right)} \quad (7)$$

$$\dot{W}_{elec} = IU \quad (8)$$

$$i_0 = i_0^{ref} a_c L_c \left(\frac{P_r}{P_r^{ref}}\right)^{\gamma} e^{-\frac{E_c}{RT}\left(1-\frac{T}{T_{ref}}\right)} \quad (9)$$

Equations (1) and (2) define the basic current and open cell voltage parameters as a function of the basic thermodynamic parameters. Equations (3) through (6) are basic definitions of fundamental loss mechanisms in the fuel cell. Finally, equations (7) to (9) relate parameters within the loss equations to the physical (1D) parameters in the fuel cell model.

Analysis of a singular fuel cell reveals that the model predicts, as expected, that it is possible to enhance the power and efficiency of the fuel cell with certain thermodynamic parameters, but as more current is drawn for a certain fuel cell area, the concentration and depletion of reactants in the gas diffusion and catalyst layer becomes less important and simply the effective area and capability of the membrane to pass a current density incurs excessive losses. That is to say, as stack pressure increases, the concentration of reactants at the membrane will also increase, and thus the capability of the membrane to pass a particular current density becomes the major limiter in fuel cell power output. Thus, as we will see, there is, as we wholly expect, a limit to how much power density can be extracted out of a fuel cell even when the system is able to optimize thermodynamic parameters.

2.2 1D Fuel Cell Design Parameters

A baseline model of the PEMFC was initially generated. Physical parameters for this model are provided in **Table 1**. Based on the power curve of this fuel cell, shown in **Figure 1**, an operating current of 1950 A (current density of 6500 A/m^2) was selected as the operating point. Note that this operating current is below the current at peak power. The entire fuel cell is comprised of 300 individual cells.

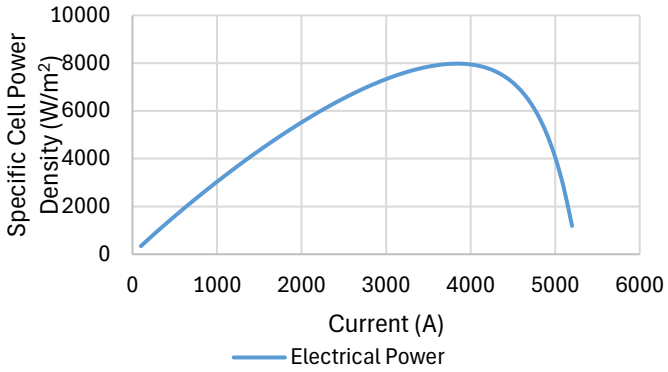

FIGURE 1: SPECIFIC CELL POWER CURVE

TABLE 1: PARAMETERS OF BASELINE PEMFC MODEL

Parameter	Value
Fuel Cell Area [m^2]	0.3
Catalyst Specific Area [cm^2/mg]	1000
Catalyst Loading [mg/cm^2]	0.5
Membrane Humidity	14
Membrane Thickness [μm]	178
Current [A]	1950
Number of Cells	300

Catalyst specific area is a property of Platinum (Pt) catalyst solids and is defined as the total surface area of the catalyst per unit mass. Several catalyst specific areas were explored up to the theoretical limit of 2400 cm^2/mg [3]. **Figure 2** shows that specific electric power density increases with catalyst specific area. State-of-the-art catalysts have a catalyst specific area around 600-1000 cm^2/mg [3]. During operation the PEMFC catalyst-specific area decreases due to Pt agglomeration and detachment.

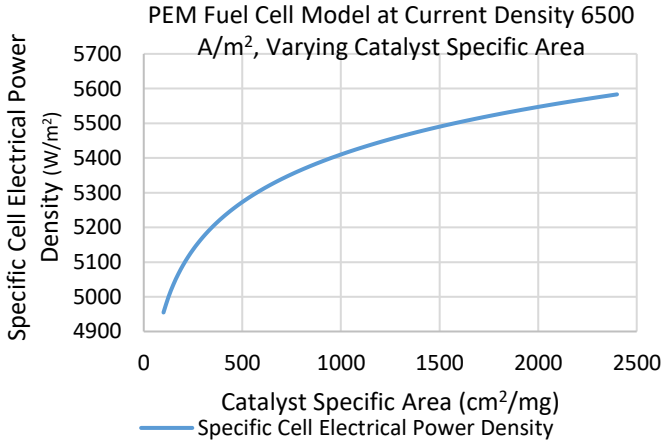

FIGURE 2: EFFECT OF CATALYST SPECIFIC AREA ON FUEL CELL POWER DENSITY

Cathode catalyst loading describes the amount of Pt catalyst per area of the cathode. **Figure 3** indicates that increasing the catalyst loading in the cathode increases the electrical power density. State-of-the-art cathodes have a loading of 0.3-4

mgPt/cm^2 [16]. Fuel cell electrode vendors offer electrodes with various catalyst loading values, so varying the catalyst loading parameter in the model represents selecting a different electrode for the construction of the PEMFC. In practice, PEMFC catalyst loading decreases over time due to electrochemical corrosion of the carbon base, causing Pt detachment and practically limiting the amount of catalyst loading. Anode catalyst loading (not shown) is typically 0.3-0.7 mgPt/cm^2 [17] and increasing it has no significant effect on power density.

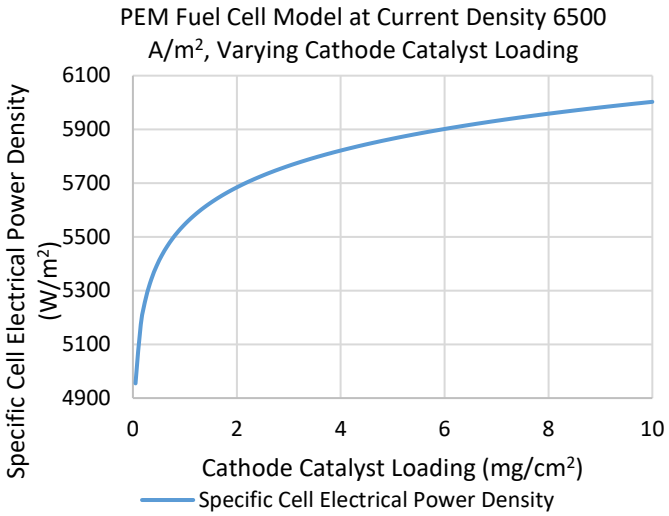

FIGURE 3: EFFECT OF CATHODE CATALYST LOADING ON FUEL CELL POWER DENSITY

Membrane humidity (λ) describes the humidity percentage in the membrane (molecules of water to molecules of sulfonic acid). Typical ranges go between 14 (considered 100% humidified) and 23 (considered flooded). **Figure 4** highlights that higher membrane humidities results in higher electrical power density. In practice, this trend works up until the membrane is 100% humidified (indicated by the dashed line), as higher humidity values mean water accumulates on the catalyst, which has a negative effect on mass transfer. Also, while the PEMFC model requires a membrane humidity value to be specified by the user, practically the water content will vary based on several operation parameters of the PEMFC (air stoichiometry, temperature, current density, etc.).

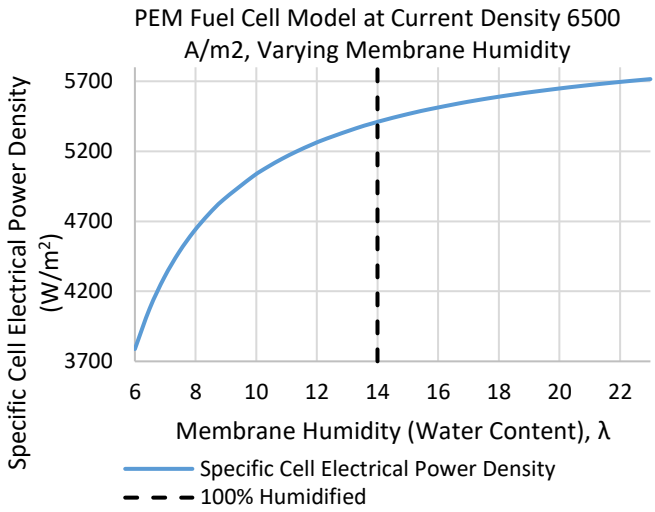

FIGURE 4: EFFECT OF MEMBRANE HUMIDITY ON FUEL CELL POWER DENSITY

Membrane thickness describes the thickness of the Nafion cation exchange membrane and is one of the main parameters for PEMFC optimization. **Figure 5** shows that electrical power density decreases with increasing membrane thickness. In practice, reinforced thin (25 or 50 μm) Nafion XL membranes with chemical stabilizers are being studied to help boost PEMFC electrical power density [3].

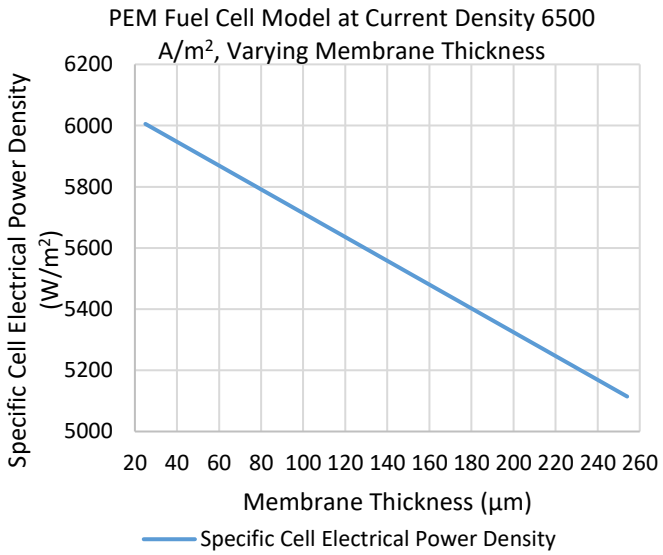

FIGURE 5: EFFECT OF MEMBRANE THICKNESS ON FUEL CELL POWER DENSITY

2.3 Determination of Baseline System

It should be established that the operation of the fuel cell proper depends upon physical parameters that are determined by the rest of the system within which the fuel cell operates. Parameters may be categorized as (i) Design, (ii) Electrical, and (iii) Thermofluid. The design parameters are those discussed in the theory description and are based on how the fuel cell is designed and constructed, such as the effective surface area,

catalyst loading, etc. The electrical parameters relate to the load control at the fuel cell electrodes, and ultimately to the effective resistance function. When the fuel cell is used in a system with synchronous motors driven by a variable frequency drive, the response of the electronic controller may be quite complex, but ultimately results in a load resistance feedback to the fuel cell terminals that is some function of the fuel cell I-V characteristic.

The thermofluid parameters are those we are primarily focused on in this work. These parameters are the pressures, temperatures, flow rates, and reactant proportions as described by the fuel-to-oxidant equivalence ratio (ϕ). ϕ is defined as the actual fuel-to-oxidizer ratio to the stoichiometric fuel-to-oxidizer ratio, as shown in Equation 10.

$$\phi = \frac{\left(\frac{m_{H2}}{m_{ox}}\right)}{\left(\frac{m_{H2}}{m_{ox}}\right)_{st}} \tag{10}$$

As we have derived from the basic physical relationships, the fuel cell I-V characteristic and losses are directly related to the partial pressures of the reactants and the temperatures. The partial pressures are subsequently a function of the total pressure of the flows and the relative flow rate of the reactants because the partial pressure, especially of the oxidizer, drops as it diffuses through the gas diffusion layer. The amount of the partial pressure drop through the diffusion layer is therefore a function of the fuel-air equivalence ratio, as oxygen in the air is depleted at the catalyst layer and converted to water.

The equivalence ratio is used in this analysis because in practical systems more hydrogen will be flowing than what is consumed in the anode by the fuel cell, but the hydrogen will be recycled out of the excess port back into the anode inlet. Therefore, fuel-air equivalence ratio is the important parameter that impacts the relative depletion of oxygen from the oxidant (air) stream.

The temperature of the fuel cell is assumed to be constrained by the design, and we use the isothermal model of the fuel cell, which is a reasonable assumption when the reactants and equilibrium temperature of the fuel cell are approximately the same. Under these conditions, the reactants quickly equilibrate to the fuel cell temperature upon entry and contact with the bipolar plates. Conceptually, the theoretical efficiency per Equation (11) is maximized by operating at lower temperature, while the voltage characteristic (the I-V characteristic) increases voltage with higher temperature per Equation (2), so there is a competing effect that is load dependent. In practice, operating temperatures should not be minimized per Equation (11) since higher temperatures provide increased energy for chemical reactions to occur, thus reducing activation losses. In this work we relied on a PEM fuel cell model, which in typical cases is constrained to a nominal 80°C. Thus, the model was set for an isothermal temperature of 80°C.

$$\eta_{th} = \frac{\Delta G}{\Delta H} = \frac{\Delta H - T\Delta S}{\Delta H} = 1 - T\frac{\Delta S}{\Delta H} \tag{11}$$

Consequentially, for an analysis system pertinent to this work (where all design variables are held fixed), the independent parameters that may be chosen are the fuel (H_2) flow rate (assuming all fuel is consumed), the equivalence ratio (thus determining the air flow rate), and the cell reactant (fuel and air) pressure (recall we are equalizing fuel and air pressures). Note that, by energy conservation, the fuel flow rate and the condition that all fuel is consumed determines the fuel cell power (and subsequently the stack current and voltage via the electrochemical simulation integral to the analysis often described by the I-V characteristic) and efficiency, and heat losses. In a physical system, the fuel consumed would of course be governed by the electrical output control – that is, the load is the primary control in the physical system as long as H_2 is continually supplied to the anode, and the unused flow of fuel is of course then recycled. In the simulation system, it is desirable to control the fuel consumption rate for parametric analysis.

The first part of the study is to establish baseline characteristics of the representative fuel cell. A parametric analysis of the fuel cell stack was performed varying fuel consumption at various pressures. Here, only the fuel cell itself is under consideration rather than the system because it is necessary to establish the parameter limits under which the fuel cell itself can operate. The results are shown in **Figure 6** and **Figure 7** as power and efficiency curves, respectively. The latter may seem remarkably similar to an I-V characteristic, and indeed it is essentially a surrogate. Note that the hydrogen consumption rate is directly proportional to the current by charge conservation. That is,

$$I = c\,\dot{m}_{H_2} \tag{12}$$

The fuel cell efficiency is the ratio of electrical power to equivalent chemical power input as shown in Equation (13). In turn, the electrical power is the product of current and voltage while the chemical power input is the product of the fuel flow and calorific heating value. These relationships are provided in Equations (14) – (15).

$$\eta_{FC} = \frac{\dot{W}_{elec}}{\dot{W}_{chem}} \tag{13}$$

$$\dot{W}_{elec} = IV \tag{14}$$

$$\dot{W}_{chem} = H_{chv}\dot{m}_{H_2} \tag{15}$$

Consequently, by combining Equations (12) to (15), we obtain the relationship that the fuel cell efficiency is directly proportional to voltage by a factor related to the molar mass, molality, and the heating value, all of which are constants.

$$\eta_{FC} = \frac{c}{H_{chv}}\,V \tag{16}$$

Thus, both the hydrogen mass flow rate and fuel cell efficiency are scales of the electrical current and voltage respectively. Therefore, **Figure 7** is a surrogate to the classical I-V characteristic that is familiar to fuel cell practitioners. This also validates that the utilized electrochemical model behaves according to physical expectations.

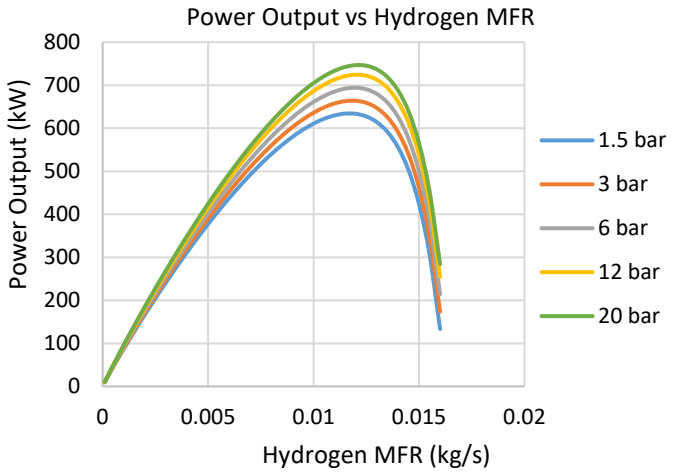

FIGURE 6: BASELINE FUEL CELL CAPACITY PARAMETRIC RESULTS OF POWER WITH VARIATION OF FUEL CONSUMPTION AND DIFFERENT STACK PRESSURES AT ϕ=0.7

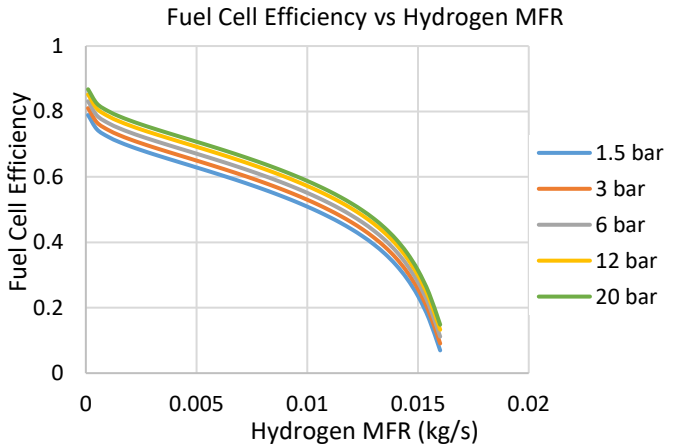

FIGURE 7: BASELINE FUEL CELL CAPACITY PARAMETRIC RESULTS OF EFFICIENCY WITH VARIATION OF FUEL CONSUMPTION AND DIFFERENT STACK PRESSURES AT ϕ=0.7

It will be noted from **Figure 6** that there is a maximum power output that may be achieved with the stack configuration under study. For any stack configuration, there will therefore be a maximum, although the maximum will depend on the design. At this point, further fuel consumption and current draw leads to voltage reduction and losses contributing to heating. Operation in this regime is generally avoided because typically electrical power production is the purpose of the system. At the same time, designs often seek to maximize the system capacity for a particular fuel cell investment, and how this may be done indeed is the central question that is highlighted in this work.

Thus, two representative operating points are selected. One at relatively low power generation and one close to the maximum. Rather than fix the power, it was decided to fix the fuel consumption at 0.004kg/s for the low power case and 0.012kg/s for the near maximum capacity case, respectively, with a focus on the latter to achieve a system that maximizes specific power density of the *fuel cell stack*. Emphasis is placed on the power density of the fuel cell stack, rather than the system. From **Figure 6** it is seen that as the stack pressure is increased, the maximum value of fuel cell stack power and the location of the maximum are both increased. It is also recognized, however, that supplying the reactants at higher pressures than ambient induces higher parasitic load on the air supply system. It can be reasonably assumed that the hydrogen fuel is already supplied by a pressurized tank, incurring no parasitic losses in pressurization. Alternatively, cryogenic liquid hydrogen would need to be pumped and vaporized; however pumping power is typically a small fraction of required compression power. Ultimately, it is therefore recognized that system architecture design has profound ramification of how the power system performs, and the cost per capacity (specific investment cost) of such a system. There may be deterioration effects that must be recognized and mitigated with this approach; however, we do not explicitly deal with this in the present work. A review of some of these issues may be found in [2] and [18].

In the following analysis, the fuel cell stack design is fixed. However, the system architecture is in variable design mode, and this point is of central relevance. Parametric exploration of several architecture and system parameters will be done to enhance our understanding of the design of a fuel cell-based power system. It is aimed to show that for certain applications where system power density is not as critical, one can produce a highly efficient and moderately economical power system. Moderately economical here is meant that there is a significant reduction in cost/net capacity ($/kW$_{net}$) by the fact that we obtain significant increase in capacity for the same fuel cell stack which represents approximately 75% of the cost of a net system and therefore achieves significant reduction in specific invenstment cost ($/kW capacity).

2.4 System Architectures

This work starts with the simply aspirated (SA) system architecture and systematically analyzes several architectures with increasing complexity. These architectures are shown in **Figure 8** - **Figure 12**. For ease of reference, the architectures are given acronym designations and enumerated as follows:

1. SA: Simply Aspirated
   This is the basic architecture that has a simple blower (with possibly an aftercooler) to supply air and a fuel cell stack to produce power.
2. PRNR: Pressure Recovery Non-Recuperated
   This system includes an expansion turbine that enables recovery of the pressure energy available at the exhaust of the fuel cell to offset the energetic cost of compression.
3. PRHR: Pressure Recovery Hot-Recuperated
   This system incorporates a recuperator that can exchange heat between the compressor discharge and recovery expander inlet, thus enabling both thermal and pressure energy recovery of the compression work.
4. PRCR: Pressure Recovery Cold-Recuperated
   An alternate variation of the PRHR system where the recuperator becomes cold, thus enabling compression

work reduction in the PRCR system instead of expansion work increase as in the PRHR system.

5. ITMR: Integrated Thermal Management Recovery
   The ITMR system is fundamentally a type of PRHR system except we envision the integration of the thermal management system with the reactant pressurization and energy recovery systems when a liquid cooled stack is utilized.

The assumptions that went into the analyses are now expounded. First, it is important to note that the analyses are fundamentally thermodynamic and electrochemical in nature, without explicit consideration of mechanical characteristics that would enable operation at various conditions (for example, the structural support of the bipolar plates to handle higher pressures and control mechanism to equalize fuel and air pressure to minimally effect membrane structure). With regard to the thermodynamics, it was conjectured that the turbomachinery and electrical machinery are optimized for the design conditions at which the analysis is made. The compressors and expanders were set for an isentropic efficiency of 85% over all analyzed pressure ratios and mass flow rates. The heat exchangers are set for either an effectiveness of 90%, or a pinch temperature of 5K (for the ITMR simulation). The fuel cell stack temperature was set to 80°C, and reactants were delivered at this temperature via thermal management controls. The parasitic load of the thermal management system was not included in the net power results but was analyzed and shown to be similar across all configurations. The ambient conditions were assumed to be 1bar and 25°C. Thus, the stack pressure expressed in bar is also the compressor pressure ratio. Pressure losses through the fuel cell gas flow channels, piping, and heat exchangers were not taken into account, as it was desired to maintain the system component design agnostic to any particular requirements.

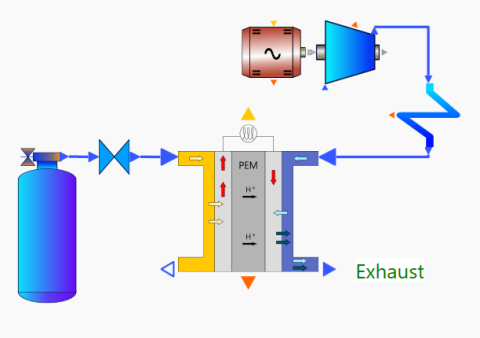

FIGURE 8: SIMPLY ASPIRATED FUEL CELL SYSTEM ARCHITECTURE

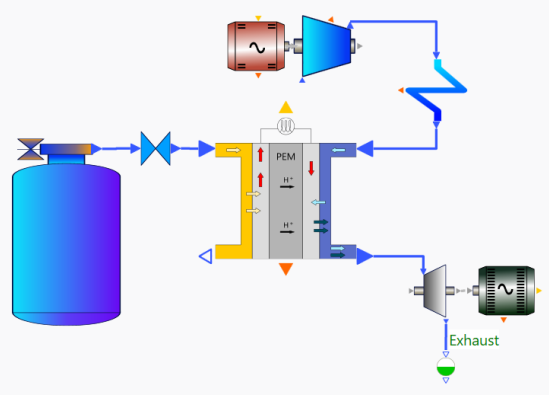

FIGURE 9: EXHAUST PRESSURE ENERGY RECOVERY WITHOUT HEAT OPTIMIZATION

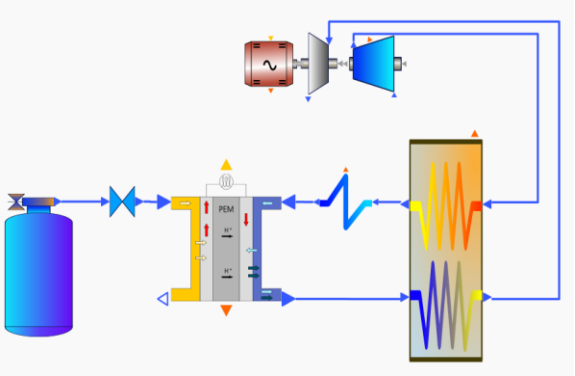

FIGURE 10: PRESSURE RECOVERY WITH RECUPERATION

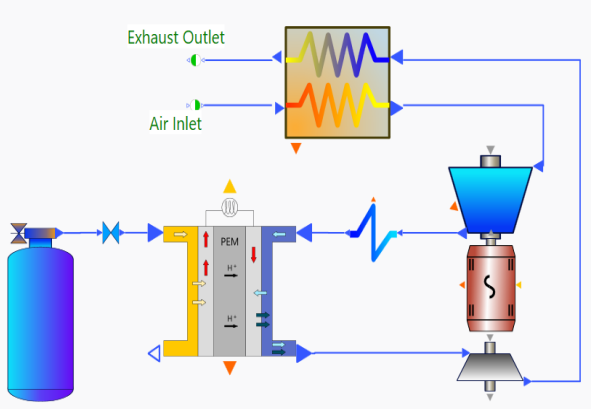

FIGURE 11: PRESSURE RECOVERY WITH COLD RECUPERATION

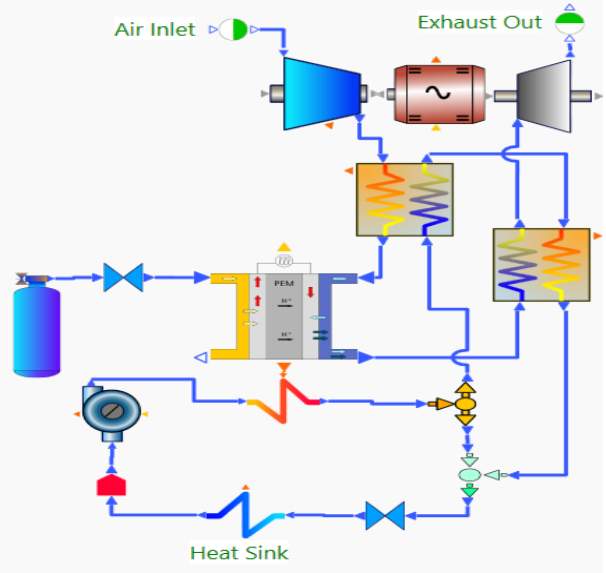

FIGURE 12: INTEGRATED THERMAL MANAGEMENT SYSTEM WITH PRESSURE RECOVERY AND RECUPERATION

The analysis proceeds by simulating each system architecture with a parametric variation of equivalence ratio (φ) and stack pressure. The stack pressure means the reactant supply pressures, with the condition that the fuel and air pressures are equalized. These are the fundamental design parameters that can be controlled at any particular design point for a fixed fuel utilization. The air and fuel systems are simulated to provide the reactants at the given design parameters for the same fuel cell configuration.

Once the operating point with peak system power is found for each system configuration, the analysis was furthered by analyzing the auxiliary power consumption of the thermal management system with the goal of verifying that it is not significantly changing. In each case, the fuel cell rejects heat to a liquid PAO coolant loop, while the heat sink of the coolant loop rejects heat to ambient air. A cooling fan was incorporated to blow cooling air across the heat sink. The configuration of the auxiliary cooling system for the first four architectures, modeled on its own, is shown in **Figure 13**, while for the ITMR architecture the auxiliary cooling system is incorporated directly into the existing thermal management system, as in **FIGURE 14**.

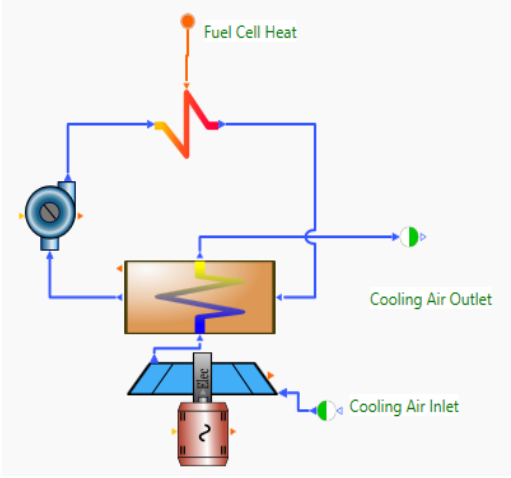

FIGURE 13: AUXILIARY COOLING SYSTEM

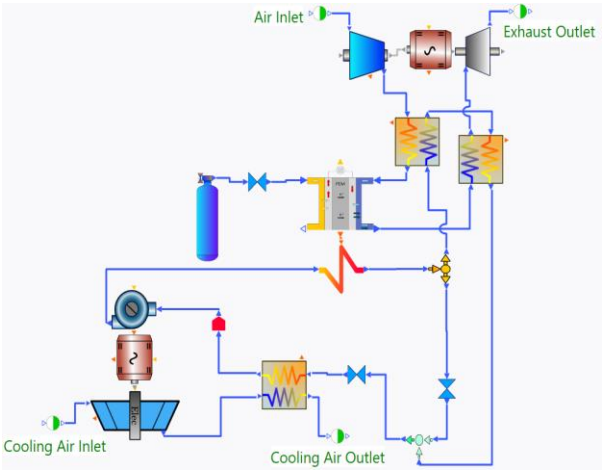

FIGURE 14: AUXILIARY COOLING SYSTEM WITH ITMR SYSTEM ARCHITECTURE

3. RESULTS AND DISCUSSION

3.1 Net System Power Results

The results of the simulations for the SA (simply aspirated) system are shown in **Figure 15** and **Figure 16** for the low power (0.004kg/s fuel flow) and high power (0.012kg/s fuel flow) cases, respectively. Although simulations for pressures beyond 5 bar were conducted, such design is outside good practice for systems without pressure recovery and therefore the results are trivial and not shown.

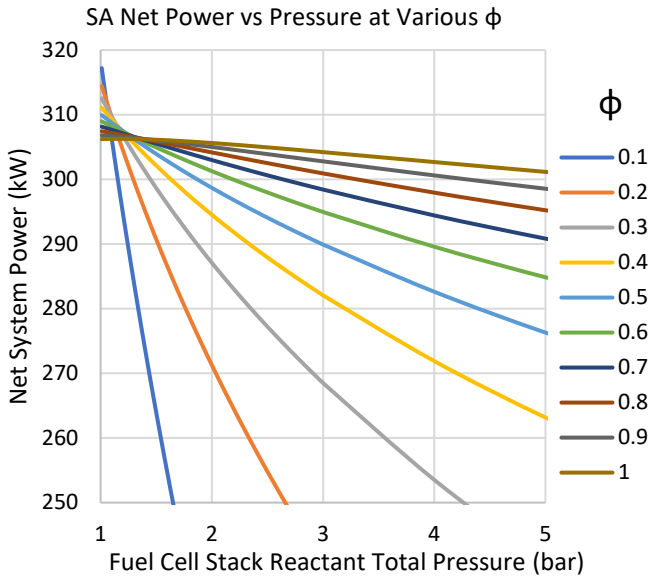

FIGURE 15: NET POWER FOR SA SYSTEM WITH LOW LOAD

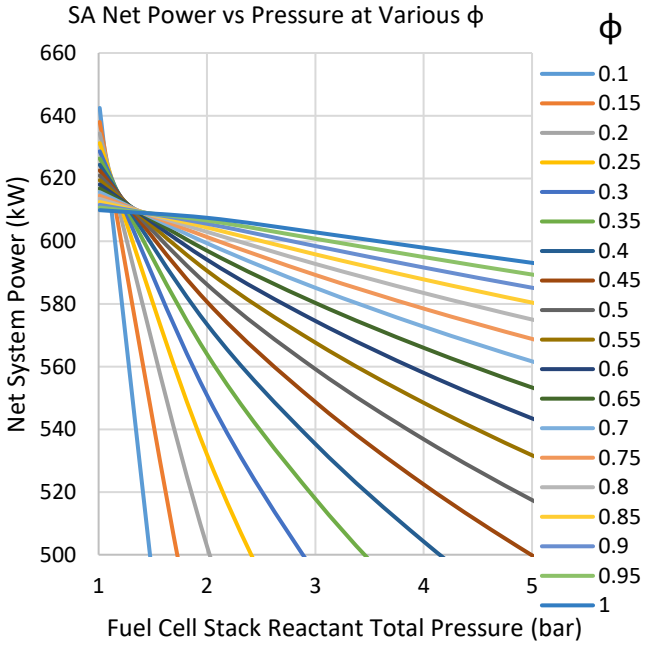

FIGURE 16: NET POWER FOR SA SYSTEM WITH HIGH LOAD

It is apparent that for practical equivalence ratios between 0.5 and 0.9 (these values are similar to those of PEMFC systems found in literature [5], [19]), the optimum stack pressure is below 1.5bar, with the optimum shifting to lower pressure ratios with more excess air (lower equivalence ratio). It is also noted that the maximum practical power for the SA system under consideration is approximately 610kW.

The results of the simulations for the non-recuperated pressure recovery system (PRNR) are presented in **Figure 17** and **Figure 18** for the respective fuel consumptions. The results are similar for both loads, with the higher load slightly more optimal at higher pressure. It is worth noting that while some of the analyzed stack pressures are above what is typically found in PEMFC's (one PEMFC manufacturer reports an 8 bar nominal fuel supply gauge pressure [20]) , this pressure limitation is based on the mechanical strength of the membrane and surrounding support structures. If the fuel and air pressure on both sides of the membrane are equalized, then only some additional strengthening support material is needed for the rest of the fuel cell to withstand the increased pressures (which does not lead to significant cost increase of the fuel cell).

With the consideration that the design equivalence ratios between 0.5 and 0.9 are practically realizable, it is seen that the optimum pressure ratio is between 2 and 5, respectively. It is recognized that fine-tuned control of the air supply flow rate, which essentially governs the equivalence ratio, is an engineering challenge in system design. That is, we recognize that the system will operate at variable loads and that it is therefore possible that at lower loads the equivalence ratio may tend lower than the design condition due to controllability aspects of the compressor.

To elaborate on this point, when load is reduced there are two limiting cases at which the system could operate. The first case is to reduce the air flow rate to maintain the same equivalence ratio at this low load (lower fuel flow rate) case. For the compressor (assumed to be a centrifugal machine) to deliver the lower flow rate of air efficiently, it will need to operate at reduced speed and reduced pressure ratio, thus reducing the fuel cell stack pressure. For system architectures with a turbine, since the flow parameters through the turbine will be adjusted for this low load case, the performance of the turbine (with fixed geometry) can also be expected to vary. To maintain power recovery across the turbine at off-design operation, a variable geometry machine may be needed. The second limiting case is to maintain the same air flow rate and pressure ratio, causing a reduction in equivalence ratio. While the fuel cell efficiency increases slightly due to the increased oxygen concentration, the compressor power consumption is the same as for the high power case (therefore larger relative to the first limiting case). Additionally, the higher flow rate naturally leads to increased pressure losses along the air fluid and piping lines. Somewhere between these two limiting cases will be an optimum operating case which maximizes system efficiency at low loads, constrained of course by the limitations of the compressor. Such an optimization would be performed once a detailed design of system components is finished and is not the scope of the present work. One can therefore see how at low loads the system may operate at lower equivalence ratios than the design condition, and therefore why low equivalence ratios are shown.

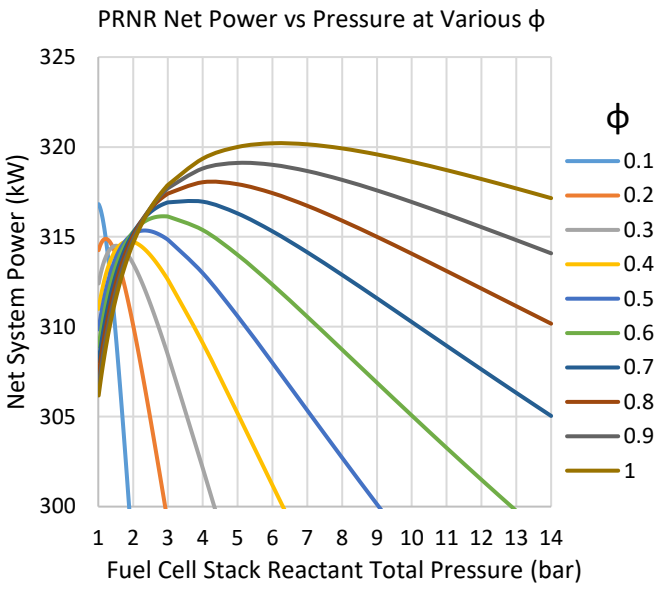

FIGURE 17: NET POWER FOR PRNR SYSTEM WITH LOW LOAD

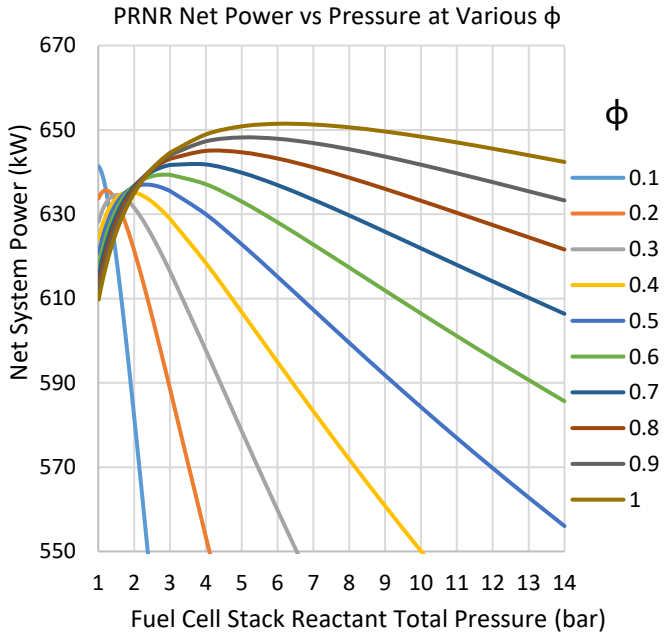

FIGURE 18: NET POWER FOR PRNR SYSTEM WITH HIGH LOAD

It will be noted that since no recuperating heat exchanger is used in the PRNR system, the additional weight of adding a turboexpander is marginal, particularly if that turboexpander is on the same shaft as the compressor and therefore reduces the motor work required. However, it will also be noted that with higher pressure ratios, the compressor outlet temperature increases and more aftercooling is physically required to maintain a design 80°C fuel cell inlet temperature. Finally, it is noted that practical peak power output is approximately 645kW, as compared to 610kW for the SA system. Thus, approximately 5% peak capacity and efficiency gain was realized. The capacity increase potentially lowers the capital cost per kW, while the efficiency of course lowers operating cost and total cost of ownership.

Figure 19 and **Figure 20** show the resulting parametric simulations of the PRHR power system, the system that incorporates a recuperator that transfers thermal energy between the compressor outlet and the recovery turbine inlet. This system mitigates the compression work penalty as most of it can be recovered, minus any losses in the turbomachinery.

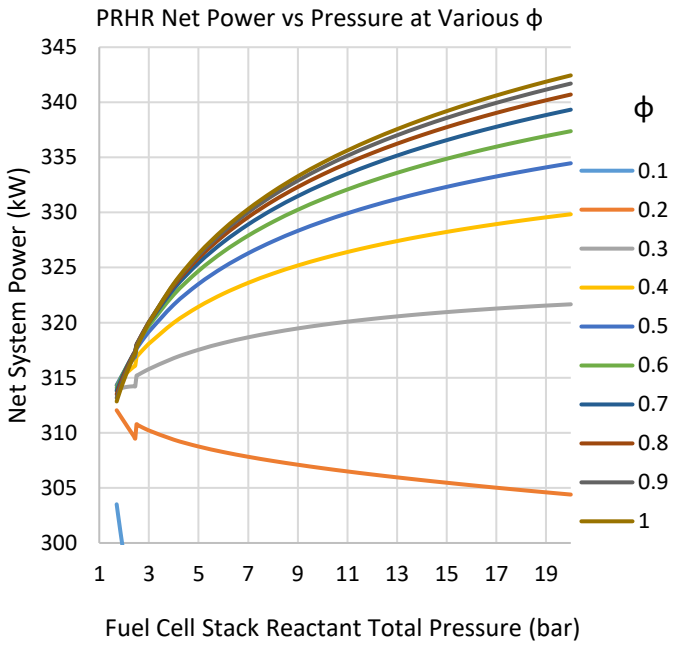

FIGURE 19: NET POWER FOR PRHR SYSTEM WITH LOW LOAD

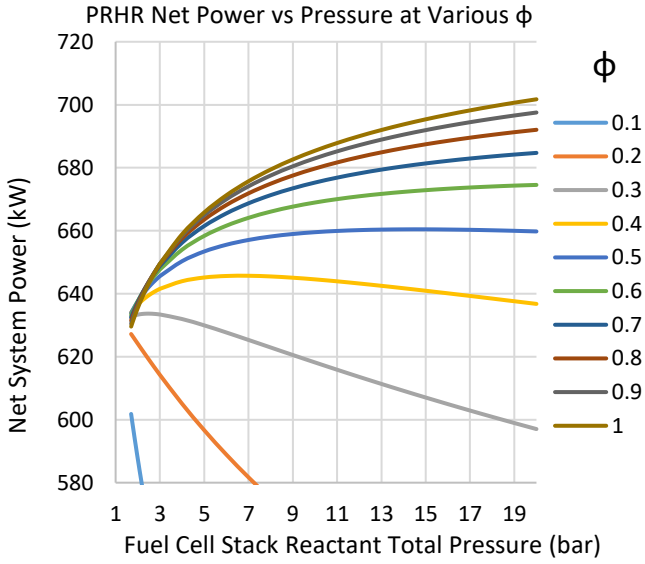

FIGURE 20: NET POWER FOR PRHR SYSTEM WITH HIGH LOAD

Unsurprisingly, the result is seen as shifting the optimum pressure ratio toward quite high values. Indeed, with equivalence ratios of 0.6 and above, it is seen that pressure ratios higher than 20 may further improve system capacity and efficiency, although we are not aware of stacks that are designed to handle such high pressures. The maximum power is approximately 700kW, achieving approximately 15% relative increase in system capacity and efficiency.

The simulation results of the PRCR system are shown in **Figure 21** and **Figure 22** for low and high loads, respectively. Fundamentally, the PRCR system is fairly similar to PRHR except that the recuperation is on the low temperature side. The drawback of this system is its limit of application to fuel cells that are able to operate at higher temperatures. This limitation is a consequence of the triple point of water near 0°C. For high pressure ratios (~10), an 80°C turbine inlet would result in very cold (about -60°C) temperature and therefore frosting issues in a cold recuperation system. However, if a high temperature PEM fuel cell were used where the allowable temperature is 200°C [21], a pressure ratio of 10 would result in about 6°C turbine outlet and therefore is a realistic operating point that would not encounter issues with exhaust vapor frosting. From this perspective these results will still generally apply to higher temperature stacks, even though the analysis was performed with parameters of a typical PEM system with 80°C temperature. It is seen that a significant improvement in capacity and efficiency, close to that of a PRHR system, is still possible. Such configurations may be of high importance when it is considered that it may be possible to replace the thermal management system with a controlled application of a PRCR system where the equivalence ratio is determined by cooling requirements. Although such a system may not achieve the maximum capacity or efficiency, its overall system power density in balance with a low specific cost may make such a system an optimal choice in certain markets and applications.

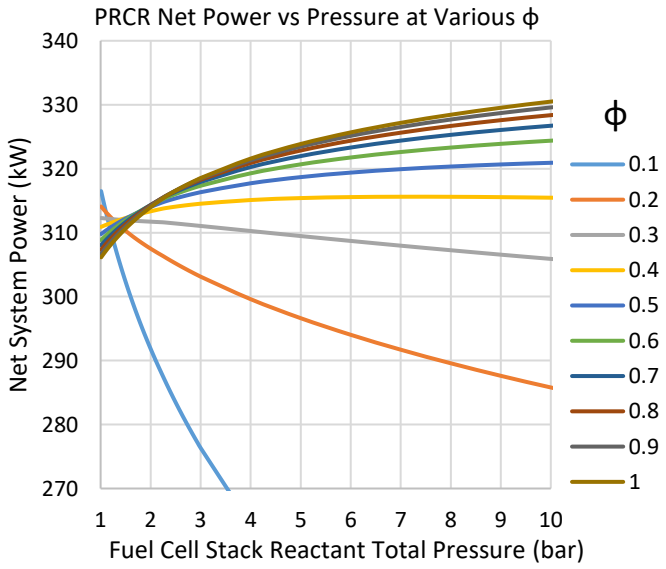

FIGURE 21: NET POWER FOR PRCR SYSTEM WITH LOW LOAD

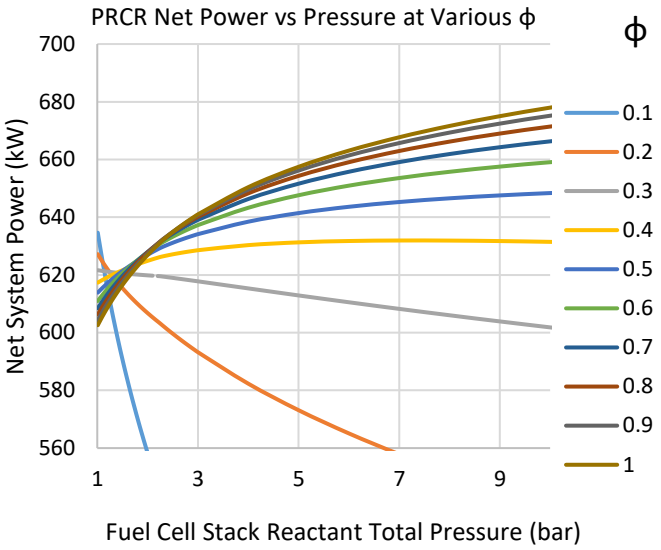

FIGURE 22: NET POWER FOR PRCR SYSTEM WITH HIGH LOAD

Finally, the results of the ITMR system parametric simulations for low and high loads are shown in **Figure 23** and **Figure 24**. The ITMR system is fundamentally a type of PRHR system with integrated thermal management and recuperation. As is seen, the results are fairly similar to the PRHR system. As a consequence of the modeling method, the heat exchangers of the ITMR system were modeled with a pinch temperature of 5K, whereas the other systems' heat exchangers were modeled with an effectiveness value of 90%. The effective pinch at high pressures resulted the ITMR system having a better heat transfer effect compared to the PRHR system. However, it must be noted that this is likely only a result of the assumptions rather than a fundamental result. It is seen that the ITMR system can perform exceptionally well and achieve the enhancement in efficiency and capacity seen in the PRHR system.

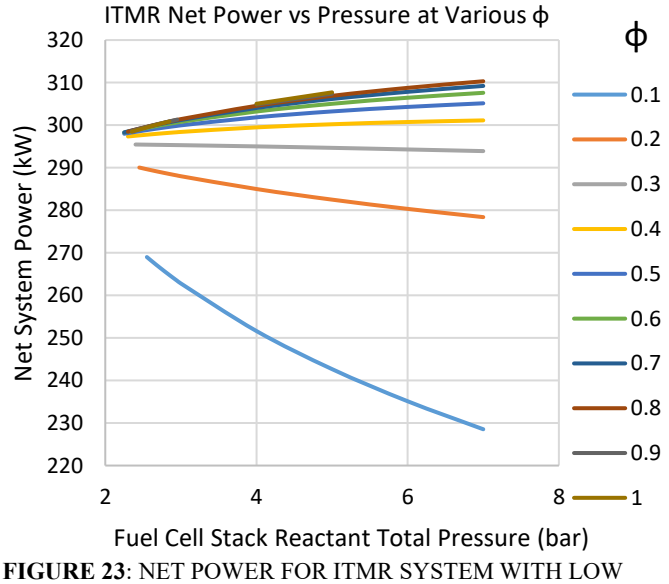

FIGURE 23: NET POWER FOR ITMR SYSTEM WITH LOW LOAD

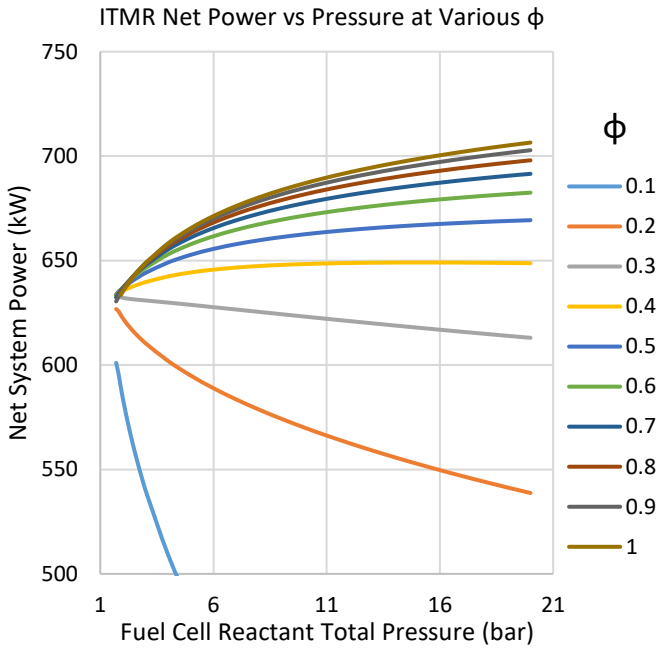

FIGURE 24: NET POWER FOR ITMR SYSTEM WITH HIGH LOAD

In order to enhance the comparison of the five system architectures investigated here, **Figure 25** - **Figure 28** are presented below to compare the maximum net system power across the entire pressure range, zoomed in to a lower pressure range, and the system efficiency, respectively.

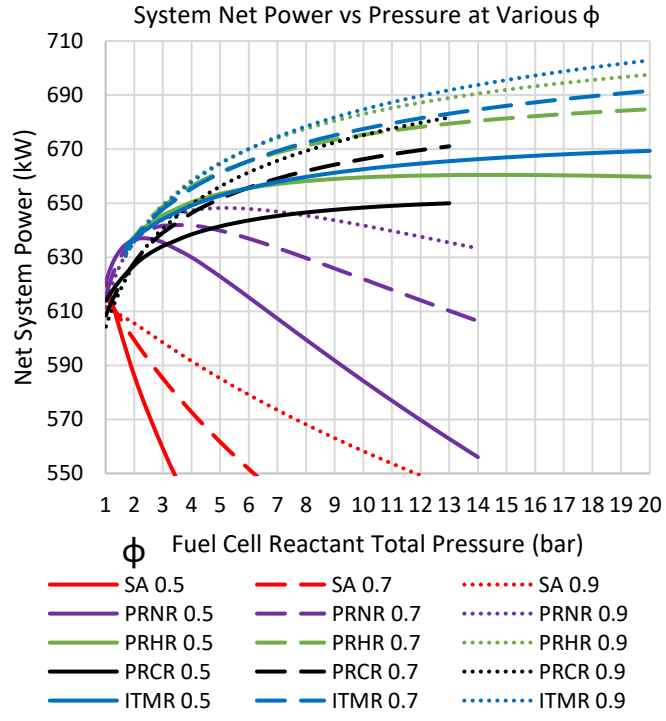

FIGURE 25: NET POWER FOR ALL FUEL CELL SYSTEMS AT HIGH LOAD FOR MULTIPLE EQUIVALENCE RATIOS

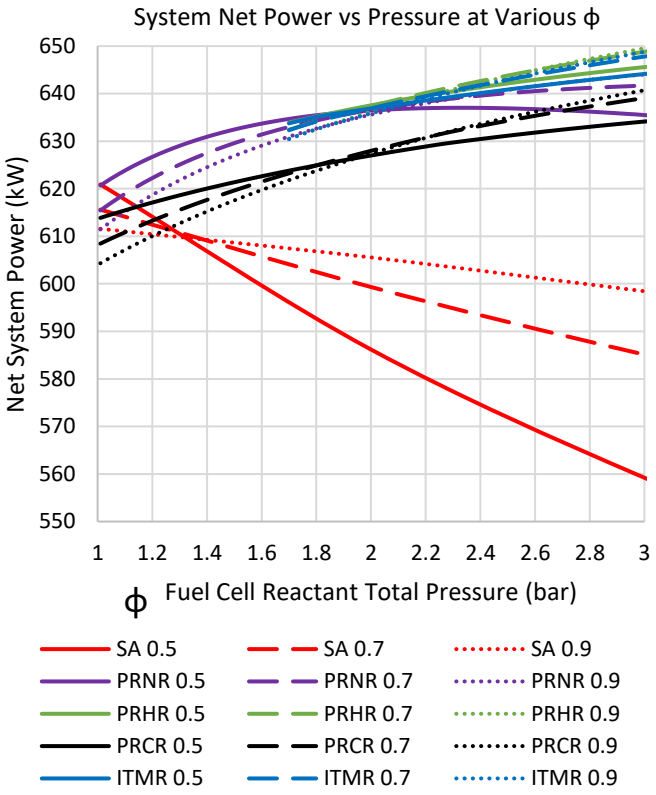

FIGURE 26: NET POWER FOR ALL FUEL CELL SYSTEMS AT HIGH LOAD FOR MULTIPLE EQUIVALENCE RATIOS (LOW PRESSURES)

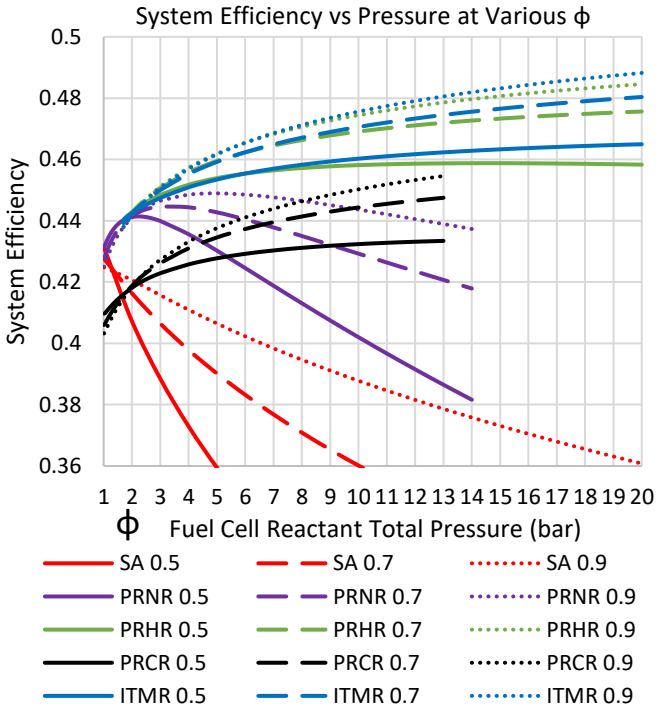

FIGURE 27: SYSTEM EFFICIENCY FOR ALL FUEL CELL SYSTEMS AT HIGH LOAD FOR MULTIPLE EQUIVALENCE RATIOS

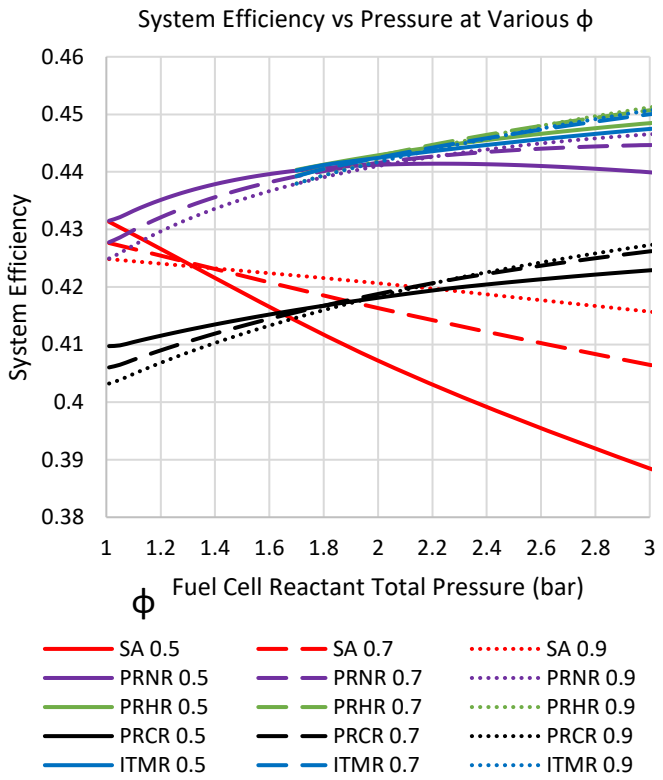

FIGURE 28: SYSTEM EFFICIENCY FOR ALL FUEL CELL SYSTEMS AT HIGH LOAD FOR MULTIPLE EQUIVALENCE RATIOS (LOW PRESURES)

3.2 Peak System Power Results Summary

A summary of the optimum results of each system is shown in **Table 2**. We can see that a significant enhancement in system performance can be attained by optimizing the system design relative to the baseline simply aspirated (SA) system.

TABLE 2: OPTIMUM RESULTS SUMMARY

System	SA	PRNR	PRHR	PRCR	ITMR
Peak System Power (kW)	614	648	697	682	703
High Load Peak Efficiency	42%	45%	48%	45%	49%
Part Load Peak Efficiency	63%	66%	71%	69%	68%

At the peak power operating point for each system architecture, the effect of the auxiliary cooling system (ACS) on net system power was analyzed. The coolant loop utilized PAO with 1 bar of pressure rise across the coolant pump. The heat sink was cooled by ambient air. It was assumed that a 500 Pa pressure rise is necessary from the cooling air fan to move the air through the pressure drop of the heat sink radiator. The cooling air was assumed to be heated from 25 °C (ambient) to 35 °C across the heat sink in each case. Based on the cooling air temperature rise and the heat transfer across the heat sink, the cooling air mass flow rate was calculated. An 85% internal efficiency and 98% drive efficiency was assumed for both the fan and the pump. The hot and cold temperatures of the PAO at the fuel cell and the heat sink were assumed to be 60 °C and 40 °C respectively. Based on the heat load from the fuel cell and the hot PAO temperature, the flow rate of the PAO was calculated. Based on these assumptions, the optimum system results can be adjusted as in **Table 3**.

TABLE 3: OPTIMUM RESULTS SUMMARY WITH AUXILIARY COOLING SYSTEM

System	SA	PRNR	PRHR	PRCR	ITMR
Peak System Power, No ACS (kW)	614	648	697	682	703
ACS Pump Power (kW)	2.8	2.5	2.3	2.6	2.3
ACS Fan Power (kW)	41	37	34	38	35
Total ACS Power (kW)	43.8	39.5	36.3	40.6	37.3
Fraction of System Power	7%	6%	5%	6%	5%

One should note that the system configurations with higher power densities have lower heat rejection from the fuel cell, and thus lower cooling requirements for the ACS because there is a corresponding increase in fuel cell efficiencies (recall fuel flow is a constant value in the analysis). Also of note is that the power requirement of the ACS is a small percentage of the peak system net power for each of the system configurations.

While the results indicate the ITMR system is that with the highest peak power, that doesn't necessarily mean it is the optimal system for all applications. Given the additional hardware required for the other systems over a simply aspirated system, these types of systems will need more space to operate and have more weight. Certain applications such as those in aerospace may consider a simpler SA system given the added weight of the other systems. Additionally, applications where space for the system is limited (such as smaller transportation vehicles) may look to go for a more compact SA system. However, stationary applications or mobile applications that can support a larger PEMFC system (such as a large truck or locomotive) would be a good choice for the higher peak power systems.

3.3 Fuel Cell System Economic Analysis

To understand the effect of different system configurations on overall system cost and the system specific investment cost (SIC), an economic analysis was performed. Here, SIC is defined as the cost per unit of net system power produced (eg. $\$/kW_{net}$). This analysis was based on previous fuel cell system economic analyses [5] as well as some assumptions on the cost distribution of the system. These cost distribution assumptions were

necessary since some of the fuel cell system components were not accounted in the present technical analysis.

Previous analyses provide a SIC breakdown of both the fuel cell stack and the balance of plant (BOP). The balance of plant is further broken down into several component groupings, including the air loop, coolant loop, and heat exchanger (compressor aftercooler). Note that not all BOP groupings were accounted in this analysis. The SIC of each of these groupings is provided in **Table 4**.

TABLE 4: COST BREAKDOWN FOR STACK AND BOP COMPONENT GROUPS [5]

Fuel Cell System Grouping	SIC ($/kW$_{net}$)
Fuel Cell Stack	$112.00
Balance of Plant	$67.00
Air Loop (BOP subgroup)	$16.08
Coolant Loop (BOP subgroup)	$14.07
Heat Exchanger (BOP subgroup)	$3.35

Furthermore, the air loop and coolant loop both consist of multiple components. The air loop consists of a compressor, expander, motor, air filter, demister, along with various smaller sensors and components. It was assumed that compressor and expander each take up 1/3 of the air loop total SIC. The coolant loop consists of a coolant pump, radiator, reservoir, filters, valves, and various smaller sensors and components. It was assumed that the coolant pump and radiator each take up 1/3 of the coolant loop total SIC. To have a congruent comparison between the SIC for the fuel cell system from literature and our analyzed systems, the SIC of all the additional miscellaneous BOP components are also included in our analysis. These miscellaneous components include additional hardware for the fuel loop, motor, motor cooling loop, sensors, reservoirs, humidifiers, system controllers, and other smaller components. Based on these assumptions, a component-level SIC breakdown is provided in **Table 5**.

TABLE 5: COST BREAKDOWN FOR FUEL CELL SYSTEM COMPONENTS [5]

Fuel Cell System Components	SIC ($/kW$_{net}$)
Fuel Cell Stack	$112.00
Compressor	$5.36
Turbine	$5.36
Coolant Pump	$4.69
Radiator	$4.69
Aftercooler	$3.35
Recuperator	$3.35
Miscellaneous BOP Components	$44.22

Based on the SIC of each component and the net system power for each system configuration, the cost of each component was calculated. There are a few special cases that should be highlighted. First, the fuel cell cost was calculated based on the fuel cell stack SIC and net system power for the SA system configuration. Because the fuel cell parameters did not change between system configurations, the fuel cell cost was assumed to be constant for each system configuration. Second, the costs of certain components are set to zero if they are not present in the particular system configuration. Third, it was assumed that the ITMR system configuration had no aftercooler and two recuperators. Fourth, the cost of miscellaneous BOP components was assumed to be the same for all system configurations, with the baseline cost calculated based on the PRNR system. Lastly, the cost of the turbomachinery and heat exchangers were assumed to grow based on their power consumption or heat transfer, respectively. The scaling of these costs was based on a logarithmic model found in literature [22] which was tuned for the system size considered in the present work. Based on these assumptions, the component costs for each system configuration are provided in **Table 6A** and **Table 6B**.

TABLE 6A: SYSTEM COST FOR EACH SYSTEM CONFIGURATION

System	SA	PRNR	PRHR
Fuel Cell	$68,768	$68,768	$68,768
Compressor	$1,439	$1,839	$2,458
Turbine	$0	$1,747	$2,333
Coolant Pump	$1,391	$1,389	$1,388
Radiator Fan	$1,505	$1,485	$1,470
Radiator	$2,345	$2,213	$2,092
Aftercooler	$851	$1,177	$926
Recuperator	$0	$0	$1,735
Miscellaneous Components	$28,654	$28,654	$28,654
Total System Cost	**$104,953**	**$107,272**	**$109,824**
System Power [kW]	614	648	697
System SIC [$/kW$_{net}$]	**$170.93**	**$165.54**	**$157.57**

TABLE 6B: SYSTEM COST FOR EACH SYSTEM CONFIGURATION

System	PRCR	ITMR
Fuel Cell	$68,768	$68,768
Compressor	$2,002	$2,458
Turbine	$1,894	$2,359
Coolant Pump	$1,390	$1,388
Radiator Fan	$1,490	$1,475
Radiator	$2,254	$2,115
Aftercooler	$1,144	$0
Recuperator	$1,039	$2,803
Miscellaneous Components	$28,654	$28,654
Total System Cost	**$108,635**	**$110,020**
System Power [kW]	682	703
System SIC [$/kW$_{net}$]	**$159.29**	**$156.50**

While the system costs are only approximate due to the assumptions made during the analysis, some trends can still be extracted from the results. As additional hardware is added to the system, the total system cost goes up. However, the systems with higher cost also have higher net system power. The trend in system SIC indicates that the increase in system power for these systems is worth the extra capital cost due to the reduction in cost per system capacity.

While various PEMFC system SICs have been reported depending on various system configurations and production volumes, one literature source reports this value at $179/kW$_{net}$ [5]. This value is comparable to the system SICs proposed in this article.

In all these systems, the fuel cell made up the majority of the total system cost. The fraction of the fuel cell cost to the total system cost ranged from 62% (ITMR configuration) to 66% (SA configuration). This value is in line with other literature studies, where the fuel cell makes up the majority of the fuel cell system cost [5].

4. CONCLUSION

Several architectures of fuel cell systems have been analyzed using the AxSTREAM System Simulation software that utilizes a lumped-parameter 1D approach to modeling the system. It is seen that with appropriate system design, the specific power and power density of the fuel cell proper can be greatly enhanced. We see, for example, approximately a 15% increase in peak power and efficiency from SA systems to PRHR systems.

Such an enhancement may be necessary to enable penetration into certain markets. We recognize that many challenges may exist with running a fuel cell at high power density and high pressures. Of course, one of the key challenges in running a fuel cell at high pressure is ensuring the differential pressure across the MEA does not damage the membrane. Another key challenge is ensuring sufficient cooling.

We are confident that both challenges can be surmounted with appropriate design. For example, to mitigate concerns with pressure damage to the MEA, a regulation system may be incorporated to ensure the reactant pressures are equalized across the membrane. Additionally, structural support can be incorporated into the design. Critically, we will recognize that these features are suitable to low cost when economies-of-scale principles are incorporated in a serialized product. This is in contrast to the catalyst material and the membrane, which fundamentally cannot benefit from cost optimizations when scaled up.

Thus, by incorporating the system design approach that minimizes capital cost and operational cost through efficiency improvement, fuel cell power systems may be more easily adopted in cost-sensitive industries where size and weight are not primary concerns.

ACKNOWLEDGEMENTS

The authors would like to acknowledge the work of Oleksandr Brovin, who was the technical leader for developing the electrochemical model of the PEM fuel cell in AxSTREAM System Simulation and continues to develop advanced models within the program for other electrochemical components. We also acknowledge the troubleshooting in System Simulation done by Serhan Memuk and some of the preliminary analysis. Finally, the work could not have been accomplished without the support of SoftInWay on developing the code and sponsoring the R&D activities.

REFERENCES

[1] C. Soares, "Gas Turbines in Simple Cycle Mode Introduction," [Online]. Available: https://netl.doe.gov/sites/default/files/gas-turbine-handbook/1-1.pdf. [Accessed 4 January 2024].

[2] L. Fan, Z. Tu and S. H. Chan, "Recent Development of Hydrogen and Fuel Cell Technologies: A Review," *Energy Reports,* vol. 7, pp. 8421-8446, 2021.

[3] F. Barbir, PEM Fuel Cells: Theory and Practice, Academic Press, 2012.

[4] J. D. Nicholas, "Highlights from the 2013 National Science Foundation Solid Oxide Fuel Cell Promise, Progress, and Priorities (SOFC-PPP) Workshop," *The Electrochemical Society Interface,* vol. 22, no. 4, p. 49, January 2013.

[5] G. Kleen, W. Gibbons and J. Fornaciari, *DOE Hydrogen Program Record #23002,* Washington DC: US Department of Energy, 2023.

[6] P. N. Papadopoulos, A. G. Marinopoulos and G. K. Papagiannis, "PEM Fuel Cell Model in the Simulation of a Distributed Generation Network," 2008.

[7] C.-Y. Wang, "Fundamental Models for Fuel Cell Engineering," *Chemical Reviews,* vol. 104, no. 10, pp. 4727-4766, 2004.

[8] A. Omran, A. Lucchesi, D. Smith, A. Alaswad, A. Amiri, T. Wilberforce, J. R. Sodré and A. Olabi, "Mathematical model of a proton-exchange membrane (PEM) fuel cell," *International Journal of Thermofluids,* vol. 11, 2021.

[9] M. Hübel, N. Nirmala, M. Deligant and L. Li, "Hybrid Physical-AI Based System Modeling and Simulation Approach Demonstrated on an Automotive Fuel Cell," in *Modelica Conferences*, 2022.

[10] D. D. Boettner, G. Paganelli, Y. G. Guezennec, G. Rizzoni and M. J. Moran, "Proton Exchange Membrane Fuel Cell System Model for Automotive Vehicle Simulation and Control," *Journal of Energy Resources Technology,* vol. 124, no. 1, pp. 20-27, 2002.

[11] R. B. Mejías, C. A. Saias, I. Roumeliotis, V. Pachidis and M. Bacic, "Assessment of Hydrogen Gas Turbine-Fuel Cell Powerplant for Rotorcraft," *International Journal of Hydrogen Energy,* vol. 50, pp. 772-783, 2024.

[12] S. M. C. Ang, E. S. Fraga, N. P. Brandon, N. J. Samsatli and D. J. Brett, "Fuel cell systems optimisation - Methods and strategies," *International Journal of Hydrogen Energy,* vol. 32, no. 22, pp. 14678-14703, 2011.

[13] T.-K. Yeh and C.-H. Chen, "Modeling and optimizing the performance of a passive direct methanol fuel cell," *Journal of Power Sources,* vol. 175, pp. 353-362, 2008.

[14] Y. Zhao, N. Shah and N. Brandon, "The Development and Application of a Novel Optimisation Strategy for Solid Oxide Fuel Cell-Gas Turbine Hybrid Cycles," *Fuel Cells,* vol. 10, no. 1, pp. 181-193, 2010.

[15] SoftInWay Inc., "Fuel Cell PEM Electrochemical Isothermal," [Online]. Available: https://wiki.softinway.com/id/5869/net-fuel-cell-pem-electrochemical. [Accessed January 2024].

[16] D. V. Nolasco, "Optimization of membrane electrode assembly for PEM fuel cells," Budapest University of Technology and Economics, Budapest, 2021.

[17] H. Tang, K. Geng, D. Aili, Q. Ju, J. Pan, G. Chao, X. Yin, X. Guo, Q. Li and N. Li, "Low Pt loading for high-performance fuel cell electrodes enabled by hydrogen-bonding microporous polymer binders," *Nature Communications,* vol. 13:7577, 2022.

[18] H. Pourrahmani, M. Siavashi, A. Yavarinasab, M. Matian, N. Chitgar, L. Wang and J. Van herle, "A Review on the Long-Term Performance of Proton Exchange Membrane Fuel Cells: From Degradation Modeling to the Effects of Bipolar Plates, Sealings, and Contaminants," *Energies,* vol. 15, p. 5081, 2022.

[19] J. M. Cunningham, M. A. Hoffman and D. J. Friedman, "A Comparison of High-Pressure and Low-Pressure Operation of PEM Fuel Cell Systems," *SAE Transactions,* pp. 464-470, 2001.

[20] Ballard Power Systems, "Fuel Cell Power for Medium Duty Applications," 2024. [Online]. Available: https://www.ballard.com/docs/default-source/spec-sheets/fcmovetm.pdf?sfvrsn=77ebc380_4.

[21] S. S. Araya, F. Zhou, V. Liso, S. L. Sahlin, J. R. Vang, S. Thomas, X. Gao, C. Jeppesen and . S. K. Kær, "A Comprehensive Review of PBI-based High Temperature PEM Fuel Cells," *International Journal of Hydrogen Energy,* vol. 41, pp. 21310-21344, 2016.

[22] M. Shamoushaki, P. H. Niknam, L. Talluri, G. Manfrida and D. Fiaschi, "Development of Cost Correlations for the Economic Assessment of Power Plant Equipment," *Energies,* vol. 14, no. 2665, 2021.